Resilience of woody ecosystems to precipitation variability

Daniella M Rempe[1a], Erica L McCormick[1a], W Jesse Hahm[2], Geeta Persad[1], Cameron Cummins[1], Dana A Lapides[2], K Dana Chadwick[1], David N Dralle[3]

[1] Jackson School of Geoscience, University of Texas, Austin, Austin, TX, USA

[2] Department of Geography, Simon Fraser University, Burnaby, BC, Canada

[3] Pacific Southwest Research Station, USDA Forest Service, Davis, CA, USA

[a] Denotes co-first author

Correspondence to: rempe@utexas.edu

This pre-print is not peer-reviewed. This pre-print was submitted to *PNAS*.

Resilience of woody ecosystems to precipitation variability

Daniella M. Rempe[a,1,2], **Erica L. McCormick**[a,1], **W. Jesse Hahm**[b], **Geeta Persad**[a], **Cameron Cummins**[a], **Dana A. Lapides**[b,c], **K. Dana Chadwick**[a], **and David N. Dralle**[c]

[a]Jackson School of Geoscience, University of Texas at Austin, Austin, TX 78712; [b]Dept of Geography, Simon Fraser University, Burnaby, BC, Canada, V5A 1S6; [c]Pacific Southwest Research Station, United States Forest Service, Davis CA 95618

This manuscript was compiled on May 20, 2022

Large-scale plant mortality has far-reaching consequences for the water and carbon cycles. The role of belowground root-zone water storage (RWS) on the conditions that lead to mortality remains uncertain. It has been proposed that the RWS capacity, S_{max}, can determine ecosystem vulnerability to drought (1, 2). However, incorporating information about RWS into prediction of vegetation dynamics has been limited due to the challenge of quantifying RWS at large scales (3, 4). Here, we present a mass-balance framework for assessing forest resilience to year-to-year variability in precipitation, including mega droughts, by quantifying RWS. We use the relationship between RWS and annual precipitation to evaluate the sensitivity of woody ecosystems to precipitation variability by classifying them as either capacity limited, where RWS is nearly constant annually and set by S_{max}, or precipitation limited, where RWS varies annually based on precipitation amount. We applied this framework to seasonally dry forests and savannas in California and found that approximately 16-23% of the state's total biomass is found in precipitation-limited locations where plants commonly rely on carryover of moisture from one year to the next. These precipitation-limited areas experienced disproportionately high rates of mortality in recent drought. In contrast, approximately 51-58% of the state's biomass is found in capacity-limited locations and thus experiences annually reliable moisture supply. Using precipitation projections for the next century, the model framework reveals a tipping point by which 5,163 km^2 (27 Tg aboveground carbon) of forest and savanna could transition from stable to unstable moisture supply. An additional 11,950 km^2 (55 Tg aboveground carbon) where moisture supply is already annually unstable is projected to experience increased water stress, due to additional years where precipitation is not sufficient to refill moisture deficits generated in dry years. This framework provides a novel approach for assessing vulnerability of RWS, and thus woody ecosystems, to climate change.

forest | climate change | root zone | tree mortality | ecohydrology

Woody ecosystems are expected to experience increases in water stress in the coming century due to projected changes in climate. To anticipate potential mortality events and associated perturbations to carbon and water cycling, an understanding of how belowground moisture stores buffer plants from meteorological drought is needed (4–6). To date, empirical and process-based modeling studies have highlighted the ecological, physiological, and subsurface conditions under which climate variability results in water stress and mortality (7–9). However, applying this understanding to real systems is difficult: few approaches exist for quantifying root-zone water storage (RWS) dynamics (3) and their impact on forest health.

Few regions are as vulnerable to projected increases in drought occurrence as Mediterranean-type seasonally dry ecosystems (10), where peak atmospheric water demand on vegetation coincides with the annually recurring dry season, amplifying the importance of RWS in determining plant water stress (1, 2, 11). Globally, areas experiencing asynchronicity in water and energy availability host some of the world's major biodiversity hotspots (10), and are projected to significantly expand in their geographic extent under future climate (12). In Mediterranean settings, like California, the two major limitations to dry season evapotranspiration (ET_{dry}) are thought to be: (1) the amount of wet season precipitation which goes into RWS and (2) the RWS capacity (here termed S_{max}) available to retain that water for use in the dry season (13). These two water supply limitations have been characterized as either "precipitation limited" or "capacity limited," respectively (1). Under capacity limitation, RWS available to plants during the dry season is limited by the RWS capacity (S_{max}). So long as net wet season precipitation exceeds S_{max}, RWS during the dry season is consistent under a large range of annual precipitation amounts. In contrast, precipitation-limited conditions are associated with large swings in dry-season RWS that depend on water year precipitation (P_{wy}) because S_{max} is large relative relative to annual precipitation. This large S_{max} could lead to a condition where water is banked during wet years and accessed for ET_{dry} in subsequent dry years.

To characterize these limitations, documentation of time-varying RWS and S_{max} is needed. However, RWS is not always well characterized by soil moisture sensing or available datasets on soil water storage capacity. Woody plants commonly access

Significance Statement

Subsurface moisture conditions strongly control how vegetation responds to drought. However, subsurface water storage is difficult to observe, confounding large-scale prediction of vegetation dynamics under variable precipitation. Here, a new framework for assessing the sensitivity of plant water use to annual precipitation (mediated by subsurface water dynamics) is applied across CA, identifying locations vulnerable to drought-induced mortality or increased water stress under projected climate change. This study provides maps of such vulnerable locations to inform forest and water resource managers and contribute to a better understanding of controls on plant water supply.

D.R., E.M., D.D. , and W.J.H conceived and designed the study, E.M. led computational data analysis with contributions from all co-authors. D.R. and E.M. led manuscript preparation, with contributions to editing from all co-authors.

The authors declare no competing interest.

[1]D.M.R. contributed equally to this work with E.L.M.

[2]To whom correspondence should be addressed. E-mail: rempe@jsg.utexas.edu

weathered bedrock for moisture in addition to soils, and this behavior is widespread across California (14–16). Geology and bedrock weathering play a strong role in determining root-zone properties such that S_{max} can be highly spatially variable (17).

Field studies that have documented RWS over time provide evidence for both capacity- (17, 18) and precipitation-limited conditions (11, 19) and reveal contrasting responses of these two categories to drought. In intensive study sites in the southern Sierra Nevada, where deep weathering leads to a large S_{max} (2), the multi-year 2012-2016 drought led to mortality (11). In these watersheds, despite the large S_{max} that allowed for carryover storage (20), forests were not resilient to multi-year drought (21). It was proposed progressive drying of RWS in the deep root-zone occurred over multiple drought years following an expansion of the canopy (also known as structural overshoot) during wet years prior to the drought (11, 22). In contrast, in the western northern California Coast Range, RWS was replenished annually throughout the 2012-2016 drought despite receiving less than half the mean annual precipitation (17). These forests did not experience significant drought stress or mortality despite the reduction in precipitation because they experienced similar dry-season RWS conditions each year (23). Building on these on-the-ground observations, Hahm et al., 2019a (1) introduced a stochastic hydrologic model for categorizing watersheds into precipitation- and capacity-limited conditions and analyzed 26 watersheds across California, demonstrating that precipitation-limited watersheds experienced drought stress in the 2012-2016 drought, while capacity-limited sites did not.

These prior analyses have been limited to individual hillslope-scale study sites or watersheds where year-to-year RWS could be estimated via watershed mass balance. Here, we harness recent advances in the estimation of RWS via deficit tracking methods (e.g. (14, 24, 25)) to extend these analyses across all of California's forest and savanna. We introduce three methods for categorizing woody ecosystems as precipitation limited or capacity limited using historical distributed hydroclimate datasets. We then use projected hydroclimate data and our estimates of S_{max} within this framework to predict how forest water stress will be distributed across California over the coming century. By identifying locations that are currently precipitation limited, and those which may experience precipitation-limited conditions in the future, we provide an assessment of future drought stress or mortality risk.

Results

Two example sites shown in Figure 1 illustrate three methods for characterizing precipitation and capacity limitation (represented by the three figure columns). At the capacity-limited location (Figure 1a-c), the correlation between water year precipitation (P_{wy}) and dry season ET (ET_{dry}) shows that ET_{dry} is consistent year-to-year and poorly correlated with P_{wy} (Method 1, Figure 1a; Spearman ρ = -0.18). The RWS deficit time series shows that deficits that are accrued in the dry season are reset every wet season and reach approximately the same maximum value every year (Method 2, Figure 1b; fractional carryover storage (C) = 0, see Methods). Finally, historical values of P_{wy} reliably exceed the root-zone water storage capacity (S_{max}) (Method 3, Figure 1c; probability of $P_{wy} < S_{max} = 0$). Even during drought years (2012-2016), precipitation is sufficient to reset deficits to zero each wet season, indicating that carryover storage is not needed to explain ET.

At the precipitation-limited location (Figure 1d-f), wetter years are associated with more ET_{dry} (Method 1, Figure 1d; Spearman $\rho = 0.76$). The deficit may not reset to zero during the wet season and can even accrue over multiple years, indicating use of carryover storage (Method 2, Figure 1e). At this site, carryover storage can account for up to 49% of S_{max}, indicating that some ET_{dry} in a given year is sourced from precipitation delivered in previous years. Indeed, the probability that P_{wy} will be less than S_{max} is 63% (Method 3, Figure 1f). At this location, there was tree mortality associated with the 2012-2015 drought (26).

Annual variability in root-zone water storage. Precipitation-limited and capacity-limited locations are mapped across California in Figure 1G-I following the three methods illustrated in Figure 1A-F. Gray areas are classified as capacity limited and warmer colors reflect degree of precipitation limitation. There is general agreement in the spatial distribution of the two limitation categories across all three approaches (Figure S3). Between 32 - 38% (35,740 - 42,320 km^2) of the area hosting woody ecosystems is precipitation limited, representing 16-23% of California above-ground carbon stocks.

Relative to forests, savannas tend to be precipitation limited: of the total forest area, only 10-25% is precipitation limited (5,000 - 12,700 km^2), while 45-49% of total savanna area is precipitation limited (28,300-30,600 km^2). Indeed, areas with more above-ground biomass tend to be more capacity limited (Figure 2a). Extremely wet and extremely dry areas tend to be associated with capacity and precipitation limitation respectively (Figure 2b), reflecting smaller variability in S_{max} relative to P_{wy}. Nearly all locations with mean annual precipitation (MAP) greater than 1250 mm/year are capacity limited and nearly all locations with MAP less than 500 mm/year are precipitation limited (Figure 2b). However, the majority of the area hosting woody vegetation occurs at intermediate MAP (500-1250 mm), where both precipitation and capacity limitation occur (Figure S5). High elevation areas (>2500 km) tend to be capacity limited; however, precipitation limitation is seen to a similar degree for all other elevations (Figure 2c). Capacity-limited behavior in high elevation or high MAP areas may reflect other limitations to ET_{dry} such as energy limitation.

Tree mortality (summed over the years 2014 to 2017) is associated with locations characterized as precipitation limited (Figure 2d). To test if the association between precipitation limitation and mortality results from using deficits calculated during the extreme 2012-2016 drought, we analyzed a shorter time series ending in 2012 and found that this association was maintained across all three methods, whereby the likelihood of precipitation limitation (by area) is higher for places that experienced high mortality (Figure S5).

Projected shifts in root-zone water supply. Precipitation-limited areas that are projected to experience an increase in the number of years where annual precipitation (P_{annual}) falls below S_{max} are shown in Figure 3a, where the color represents the number of global climate models that agree on this shift (see Methods). These areas could be considered the most vulnerable and likely to see increases in water stress. The

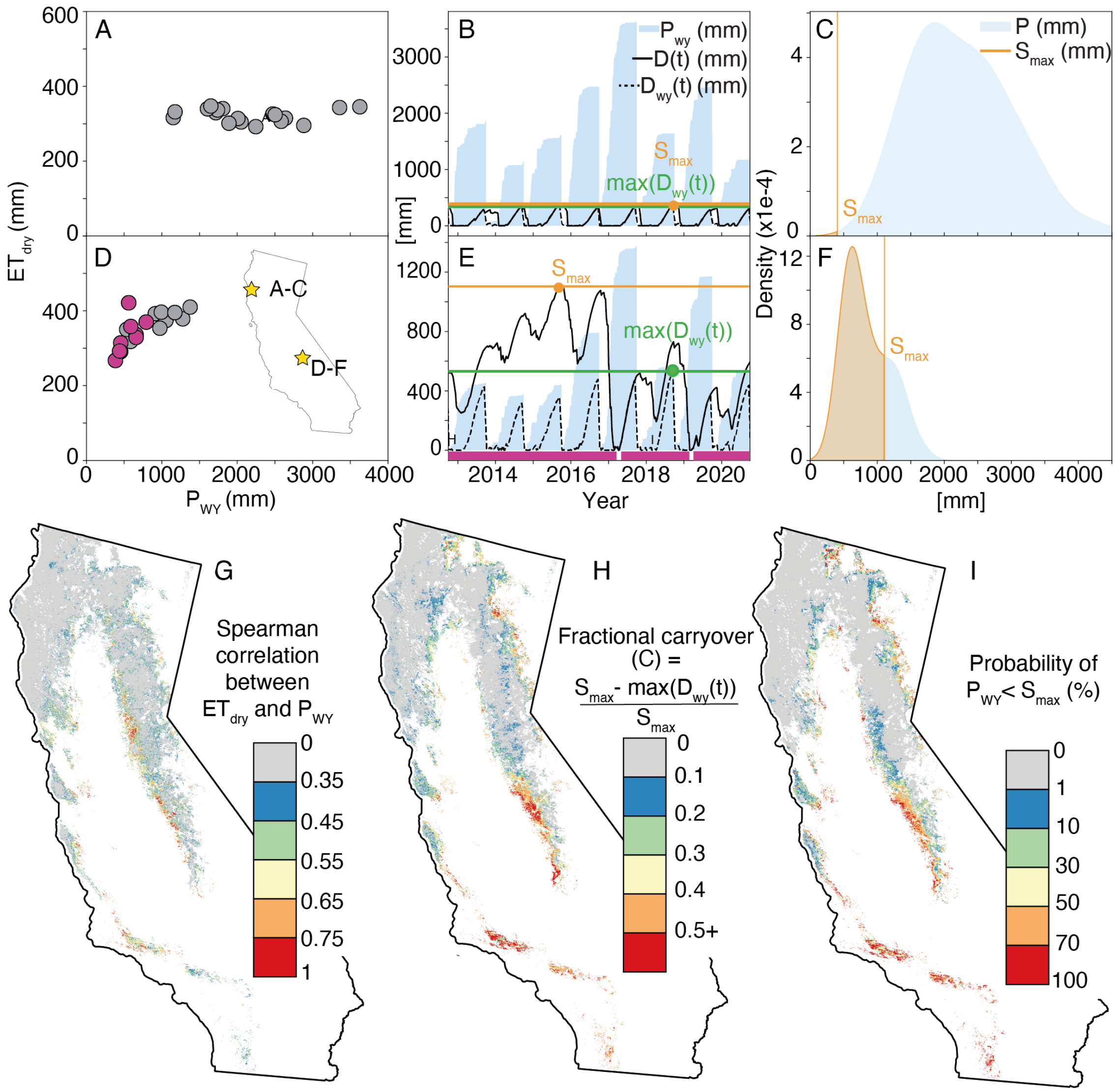

Fig. 1. Characterization of capacity-limited and precipitation-limited conditions across two sites (A-F) and California (G-I). Each vertical panel represents one of three methods (see Materials and Methods). Examples of a capacity-limited site (A-C) and a precipitation-limited site (D-F) illustrate the three methods. Locations of the two sites are shown in inset in D. From left to right: (A,D) Dry-season ET (ET_{dry}) as a function of water year precipitation (P_{wy}) for water years 2003 to 2020, where purple denotes years when carryover storage contributed to ET; (B,E) time-series of the total and water year root-zone water storage deficit ($D(t)$ and $D_{wy}(t)$) from 2012 to 2020 (full time-series shown in Figure S1). P_{wy} is shown and the minimum estimate of the root-zone water storage capacity (S_{max}, inferred from the largest observed deficit) and the maximum value of the water year root-zone water storage deficit maximums (max(D_{wy})) are highlighted with orange lines and labels. Purple bars at the bottom highlight years when the deficit did not reset to zero and carryover storage contributed to ET, with the magnitude of carryover storage (C) shown with the purple arrow, as calculated by the difference between S_{max} and max(D_{wy}); (C,F) distribution of historical P_{wy} from 1980-2020 with the minimum estimate of the root-zone water storage capacity (S_{max}) shown in orange. (G-I) Grey pixels represent capacity-limited woody vegetation as measured by each method, colored areas represent precipitation-limited woody vegetation, and areas in white are not classified as woody vegetation or are places where ET exceeds P over the study period (Figure S2). Agreement between three methods is shown in Figure S3 and S_{max} is shown in Figure S4.

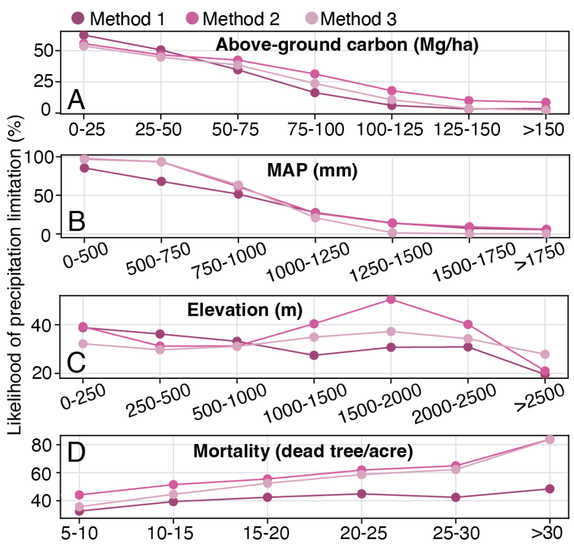

Fig. 2. The likelihood of precipitation limitation across California's woody plant communities as a function of (A) above-ground carbon, (B) mean annual precipitation (MAP), (C) elevation, and (D) tree mortality from 2014-2017. Likelihood is defined as the proportion of an area of a particular class (represented as bins on the x-axis) that is categorized as precipitation limited. In Figure S5, the areas of each bin are reported. In Figure S9, these relationships are reported for a deficit time series that ends prior to the major drought that started in 2012. Note variable y-axis limits across subplots.

11,950 km^2 area where 5 or more models agree on this shift host approximately 5% of the carbon stocks in the state (55 Tg of carbon) and nearly 11% of the woody vegetated area of the state.

For capacity-limited areas, which do not presently experience years with P_{annual} below S_{max}, we identify where projections indicate precipitation reduction below S_{max} (Figure 3b). In these areas, a transition from capacity limitation to precipitation limitation is expected and thus an increase in water stress. The 5,160 km^2 area where 5 or more models agree on this shift host approximately 3% of the carbon stocks in the state (27 Tg of carbon) and nearly 5% of the woody vegetated area of the state. Together, a total of 8% of the biomass (82 Tg of carbon) representing 16% of the forest and savanna area in the state is expected to experience increased water stress over the next century due to changes in the relationship between RWS and precipitation.

Key regions hosting biodiverse forest and savanna are projected to experience increased water stress, while some regions are projected to remain stable with respect to RWS. Substantial areas of protected land associated with national parks and forests are projected to experience an increase in water stress and/or a potential transition from capacity to precipitation limitation (Figure 3), including almost the entirely of the Sierra National Forest and Los Padres National Forest. Conversely, the majority of the northern California Coast Ranges and high elevation areas of the northern Sierra Nevada are not projected to transition from capacity to precipitation limitation conditions based on available precipitation projections. In these areas, a >40% reduction in P_{annual} during the driest years (the lowest 25th percentile of P_{annual}) would be needed to create a condition where S_{max} is not replenished (Figure S6). With respect to the role of RWS, these locations could be considered to be the least vulnerable. However, we do not account for amplified warming or decreased snow fraction, which are projected across high elevation regions and will increase reliance on RWS.

Discussion

By quantifying time varying RWS and its relationship to S_{max} and P_{wy}, we provide maps that identify where plants experience increased likelihood of experiencing water stress due to interannual variations in annual precipitation (Figure 1G-I, colored areas). Plant ecophysiology studies call for better incorporation of the subsurface to understand mortality (3). While proximate causes of mortality can be complex, water stress is considered a central prerequisite (4). Our finding that high mortality areas are more commonly precipitation limited suggests that the methods presented here could be used to fingerprint mortality risk. Methods such as (25, 27) could be used to assess S_{max} independent of observations of drought-induced deficits, to facilitate prediction of conditions outside of the range of observations.

We also report where woody ecosystems have large enough S_{max} to bank precipitation for multiple years via carryover storage (Figure 1H). In this case, large S_{max} may confer drought resilience in the sense that plants can sustain transpiration through years of drought, but it may also lead to the build-up of large root-zone storage deficits that cannot be quickly replenished, resulting in vulnerability, not resilience, to precipitation reductions in larger droughts (11, 19). Carryover storage may be the hydrological manifestation of structural overshoot by the plant community, wherein high biomass density generates storage deficits that cannot be replenished during dry years. The widespread use of carryover storage suggests that plant communities may experience other forms of limitation than water stress in the long, dry California summer, because not all water that is plant available is used in a given year. Open questions remain about the mechanisms by which water volumes unused in a previous dry season are accessed in the following year; however recent work suggests that the mechanism may be related to new root growth. For example, increased investment in belowground biomass to mine decades-old water has been reported (28).

Beyond plant vulnerability to drought, the use of carryover storage and multi-year deficit accrual associated with precipitation limitation has been linked to declines in runoff following drought (29), suggesting that watersheds with precipitation-limited areas shown in Figure 1G-I may be prone to greater hydrologic memory of drought. Understanding the relationship between RWS and precipitation variability may be key to identifying the conditions by which plant community shifts or changes to atmospheric demand impact streamflow. Improved documentation of RWS deficits and precipitation limitation can thus contribute to water resource and forestry decision making.

In both capacity-limited and precipitation-limited areas, S_{max} commonly exceeds reported values of soil water storage capacity (Figure S7). This additional root-zone water supply is routinely sourced from the underlying weathered bedrock as either rock moisture or groundwater, with the former likely being more common in California (14). Here, we exclude areas where ET exceeds P over the long term indicating a stable water source to vegetation that is decoupled from rainfall, such as lateral groundwater contribution (see Materials

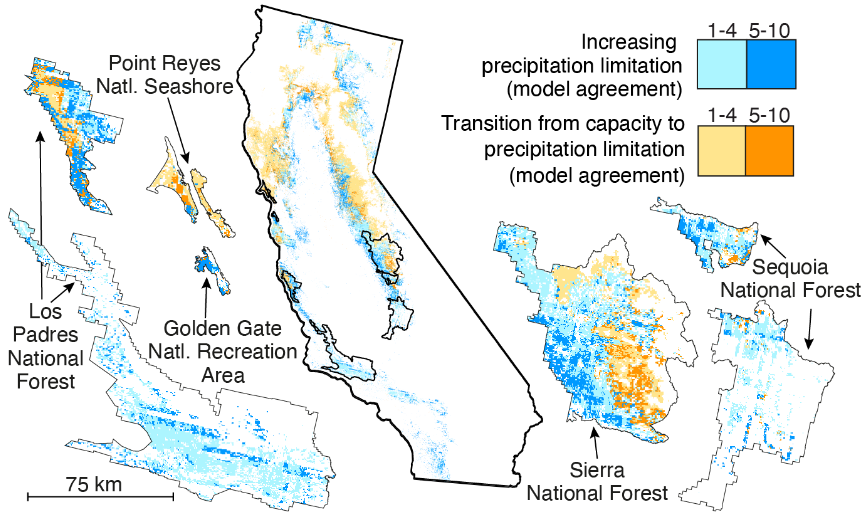

Fig. 3. Shifts in root-zone water storage (RWS) limitation for precipitation projections in 2060-2100 reflecting less favorable conditions and increased water stress. Of the area of woody ecosystems analyzed, at least 25% is projected to experience less favorable conditions. Ten climate model projections of precipitation variability are used (see Materials and Methods) to identify (in blue) locations presently characterized as precipitation limited where projected decreases in precipitation will lead to a lower probability of annual precipitation meeting or exceeding S_{max} and (in orange) locations where projected decreases in precipitation will result in a transition from capacity-limited to precipitation-limited conditions. Colors reflect the number of models that agree on the change. Pop-outs show model agreement for select national parks and forests. Scale bar refers to pop-outs.

and Methods). Such conditions, while also potentially vulnerable to projected climate change (30), are not considered here. Incorporating deeper plant-available water storage in weathered bedrock in ecohydrologic models can improve estimation of evapotranspiration under drought conditions (31). Weathered bedrock water storage dynamics are beginning to be incorporated into ecohydrologic models (32, 33) with the results presented here serving as an important constraint to such models. The geologic controls on S_{max} remain an open question, as highlighted by the large variability in S_{max} over regions receiving high precipitation (Figure S2B, Figure S4). Our assessment of S_{max} and assignment of precipitation- and capacity-limited storage at the pixel scale shows general agreement with site or watershed based assessments by previous investigators including Sequoia groves in the Sierra (20), 26 watersheds across California (1), and an evergreen forest (23) and two oak savannas (1, 19) in the northern California Coast Ranges.

Factors in addition to rainfall shortages are likely to impact future water stress; however, we focus here on interannual rainfall variability. There is a wide range in potential future annual precipitation projections for California and other Mediterranean regions, not only among GCMs but also among different future emission trajectories (34). Yet our results indicate that even in the face of this GCM range and using a relatively moderate climate change scenario (see Methods), widespread water stress increases are to be expected. Many locations hosting woody ecosystems across California are projected to experience decreases in spring precipitation, increases in temperature, increasing instances of multi-year drought, low to no snow years, and alternation between extreme wet and dry years during the next century (34–36). All of these conditions are likely to lead to greater dry season water stress attributable to longer dry periods, lower net precipitation, or increases in atmospheric demand. These additional factors, as well as the impacts of shifting species composition will be needed to determine future states of water stress (37–39).

Materials and Methods

We employ three methods (described below and illustrated in Figure 1) to classify root-zone water storage (RWS) into two categories: capacity limited and precipitation limited. We limit our analysis to forest and savanna across California at the 500 m pixel scale using the MODIS Land Cover Type dataset (40) from 2020 according to the Land Cover Type 1: Annual International Geosphere-Biosphere Programme (IGBP) classification band. Woody vegetation was defined as landcover types 1, 2, 3, 4, 5, 8, 9, corresponding to evergreen needleleaf forests, evergreen broadleaf forests, deciduous broadleaf forests, mixed forests, woody savannas, and savannas.

To quantify RWS, we rely on spatially distributed evapotranspiration (ET) and precipitation (P) datasets: the Penman-Monteith-Leunig V2 (PML) ET dataset at an 8-day resolution (41) and the Parameter-elevation Regressions on Independent Slopes Model (PRISM) (42, 43) precipitation dataset at a daily resolution. Biomass data is sourced from the 2010 above-ground carbon estimates from (44), elevation from the NASA Shuttle Radar Topography Mission (SRTM, (45)), and forest mortality from the U.S. Forest Service Forest Health Aerial Monitoring Program, which we sum over the years 2014-2017(26, 46). All data (with the exception of biomass (44, 47), forest mortality (26, 46), and bedrock water storage capacity (14)) were accessed via the Google Earth Engine (GEE) (48) Python application programming interface (API). We used GEE and the Rasterio (49), scipy (50), and xarray (51) Python packages to conduct analyses. All map figures were formatted in QGIS (52). All precipitation (whether rain or snow) is assumed to enter the root-zone. Drainage out of the root-zone need not be quantified in the approach described below, and lateral groundwater or overland flow into the pixel is assumed to be negligible (see discussion in (14, 29)).We assume that water availability rather than energy availability limits ET in the summer dry season and do not exclude any areas on the basis of energy limitation. We excluded locations where the total ET over the period from 2003 to 2020 exceeded total precipitation (see Figure S3).

To quantify RWS, we first calculate a time-varying root-zone water storage deficit ($D(t)$) following (14) and (53), which build upon (24). The deficit calculation can incorporate improved data sources as it becomes available. The root-zone water storage deficit represents the amount of water used for ET that cannot be explained by contemporaneous precipitation and therefore must result in a net drawdown of subsurface water storage. The maximum observed value of D over some time period is termed S_{max} (Eq. 1) and places a lower-bound on the true S_{max} (RWS capacity), which could be much larger but not accessed in its entirety over the study period. S_{max} is influenced by the combination of long-term processes affecting soil and bedrock water retention properties (e.g. porosity) and the contemporary ecosystem and its relationship to atmospheric water demand. For example, additional RWS may be plant-available, but if a vegetation community composition change occurred that reduced the amount of ET during dry periods (e.g. fire, mortality, land-use change), then S_{max} will be less than the actual storage capacity. We therefore assume a stable vegetation community over the period of observation. Time varying RWS can then be calculated as S_{max} less $D(t)$, under the assumptions that drainage is negligible over the time period of deficit accrual and that S_{max} reflects the actual storage capacity (see Figure S1).

In California's Mediterranean climate, the deficit is primarily accrued during the dry season, and may or may not "reset" to zero during the wet season. The deficit can therefore depend on the length of the time series analyzed. Here, we calculate S_{max} as the maximum deficit over the entire available time series (Oct. 1, 2003 to Sept. 30, 2020).

$$S_{max} \equiv max(D(t)), 2003 < t < 2020 \quad [1]$$

We also consider individual water year deficit time series, D_{wy} (Equation 2, dashed line Figure 1E), by subdividing the D time-series into water years and resetting the deficit to 0 at the start of each water year.

$$D_{wy}(t) = D(t)Oct1, (wy-1) < t < Sept30, wy; D(Oct1, (wy-1)) = 0 \quad [2]$$

where wy is water year. Although S_{max} is difficult to measure in situ, it has been estimated at several sites using neutron probes and other methods which show general agreement with the remotely sensed estimates (see Figure S1 and (14).)

Method 1: Correlation between water year precipitation and dry season evapotranspiration. Method 1 is based on (1), which categorized storage into precipitation limited and capacity limited based on the Spearman rank correlation between P_{wy} and a watershed mass-balance estimated storage on April 1. Here, we classify pixels as either precipitation or capacity limited using the Spearman rank correlation between water year precipitation (P_{wy}) and dry season ET (ET_{dry}), under the assumption that ET_{dry} scales with root-zone water storage (RWS) at the end of the wet season. A high correlation coefficient between P_{wy} and ET_{dry} (ρ approaching 1) is consistent with precipitation limitation (i.e. sensitivity of ET_{dry} to interannual variability in precipitation) and low correlation (ρ approaching 0) indicates insensitivity of ET_{dry} to precipitation consistent with capacity limitation. To define the threshold between capacity and precipitation limitation, we used the median value of ρ (0.35) across the dataset. P-values for correlations are shown in Figure S8 and correspond well to ρ indicating a significant correlation (p-value $\leq$ 0.05) in precipitation-limited locations.

Method 2: Identification of carryover storage. The objective of Method 2 is to identify locations where variability in storage year to year occurs because insufficient wet season precipitation arrives to fill deficits accrued during the preceding dry season. If the running deficit is not reset by P_{wy}, then, by mass balance, ET_{dry} may be derived from storage that arrived in a previous wet season, which we term carryover storage. Use of carryover storage is representative of precipitation limitation because it reflects year-to-year differences in RWS at the start of the dry season. Capacity-limited conditions are instead associated with low to no year-to-year variability in RWS entering the dry season.

To quantify carryover storage, we calculate the difference between S_max and the maximum deficit that can be accrued in a single water year at the site ($max(D_{wy})$). We report this value as a percentage of S_max and term it the fractional carryover storage, C. Note that carryover storage is dependant on the existence of a large enough drought during the study period to result in multi-year storage draw-down.

$$C = \frac{1}{S_{max}} * (S_{max} - max(D_{wy})) \quad [3]$$

Pixels are classified as precipitation limited if C is greater than 10% of S_max (Eq. 3).

Method 3: Comparison of annual precipitation distribution to RWS capacity, S_{max}. We classify capacity-limited conditions as pixels where net precipitation (approximated by P_{wy}) always exceeds S_{max}. Precipitation limitation, in contrast, is classified here by at least one observed value of P_{wy} falling below S_{max}, implying that storage would not be refilled in a year when P_{wy} is less than S_{max}. A percentile rank of S_{max} relative to the historical P_{wy} of greater than 0% is used to classify pixels as precipitation limited. We use the distribution of P_{wy} from 1980 to 2020. This method is based on the proposal by (1) that the relationship between S_{max} and the statistical distribution of net precipitation is a good predictor of ET_{dry} and water stress.

To assess how woody vegetation may respond to future precipitation conditions, we compare the projected distribution of annual precipitation (P_{annual}) to S_{max}. We make the assumption that S_{max} remains the same, but the distribution of P_{annual} is represented by projections of annual precipitation from 2060 to 2100 from 10 downscaled Global Climate Models (GCMs) (34, 54, 55). The 10 models were chosen by the California Climate Change Technical Advisory Group (56) as best representing the historical behavior of California-specific climate and hydrological parameters among all contemporaneous GCMs. Details on the specific GCMs, the downscaling method, and the extraction of annual precipitation can be found in (34, 54, 55). We use the same number of years as the historical analysis (n=40) and the most temporally distant available years in order to separate the past and future scenarios to allow time for the divergence of the climate regime. For the historical analysis, we use water year precipitation (P_{wy}). However, for the projections we use annual precipitation (P_{annual}) due to data availability. We use the RCP 4.5 (Representative Concentration Pathway 4.5 (57**?**)) future emissions scenario, which was developed for the Fifth Assessment Report of the Intergovernmental Panel on Climate Change (IPCC AR5) as a "medium stabilization" scenario.

Open Research. Data and code generated for this publication are available in an online data repository (https://github.com/erica-mccormick/storage-dynamics). All data and raster maps are available at https://www.hydroshare.org/resource/65b4acd080a244ef94de57c6f4e5f7d2/.

ACKNOWLEDGMENTS. The authors acknowledge funding support from the USDA Forest Service Pacific Southwest Research Station, National Science Foundation Award Number 2141763.

1. WJ Hahm, et al., Low Subsurface Water Storage Capacity Relative to Annual Rainfall Decouples Mediterranean Plant Productivity and Water Use From Rainfall Variability. *Geophys. Res. Lett.* **46**, 6544–6553 (2019).
2. PZ Klos, et al., Subsurface plant-accessible water in mountain ecosystems with a Mediterranean climate. *WIREs Water* **5**, e1277 (2018).
3. TE Dawson, WJ Hahm, K Crutchfield-Peters, Digging deeper: What the critical zone perspective adds to the study of plant ecophysiology. *New Phytol.* **226**, 666–671 (2020).
4. AT Trugman, LD Anderegg, WR Anderegg, AJ Das, NL Stephenson, Why is Tree Drought Mortality so Hard to Predict? *Trends Ecol. & Evol.* **36**, 520–532 (2021).
5. LD Anderegg, WR Anderegg, JA Berry, Not all droughts are created equal: translating meteorological drought into woody plant mortality. *Tree Physiol.* **33** (2013).
6. N McDowell, et al., Mechanisms of plant survival and mortality during drought: why do some plants survive while others succumb to drought? *New phytologist* **178**, 719–739 (2008).
7. A Porporato, E Daly, I Rodriguez-Iturbe, Soil Water Balance and Ecosystem Response to Climate Change. *The Am. Nat.* **164**, 625–632 (2004).
8. BC McLaughlin, et al., Weather underground: Subsurface hydrologic processes mediate tree vulnerability to extreme climatic drought. *Glob. change biology* **26**, 3091–3107 (2020).
9. DJ Young, et al., Long-term climate and competition explain forest mortality patterns under extreme drought. *Ecol. letters* **20**, 78–86 (2017).
10. KR Klausmeyer, MR Shaw, Climate change, habitat loss, protected areas and the climate adaptation potential of species in mediterranean ecosystems worldwide. *PloS one* **4**, e6392 (2009).
11. ML Goulden, RC Bales, California forest die-off linked to multi-year deep soil drying in 2012–2015 drought. *Nat. Geosci.* **12**, 632–637 (2019).
12. X Feng, SE Thompson, R Woods, A Porporato, Quantifying asynchronicity of precipitation and potential evapotranspiration in mediterranean climates. *Geophys. Res. Lett.* **46**, 14692–14701 (2019).
13. AW Fellows, ML Goulden, Mapping and understanding dry season soil water drawdown by California montane vegetation. *Ecohydrology* **10**, e1772 (2017) http://onlinelibrary.wiley.com/doi/abs/10.1002/eco.1772.
14. EL McCormick, et al., Widespread woody plant use of water stored in bedrock. *Nature* **597**, 225–229 (2021).
15. JH Witty, RC Graham, KR Hubbert, JA Doolittle, JA Wald, Contributions of water supply from the weathered bedrock zone to forest soil quality. *Geoderma* **114**, 389–400 (2003).
16. RC Graham, PD Sternberg, Tice, K.R., Morphology, Porosity, and Hydraulic Conductivity of Weathered Granitic Bedrock and Overlying Soils. *Soil Sci. Soc. Am. J.* **61**, 516–522 (1997).
17. WJ Hahm, et al., Lithologically Controlled Subsurface Critical Zone Thickness and Water Storage Capacity Determine Regional Plant Community Composition. *Water Resour. Res.* **55**, 3028–3055 (2019).
18. WJ Hahm, DM Rempe, DN Dralle, TE Dawson, WE Dietrich, Oak Transpiration Drawn From the Weathered Bedrock Vadose Zone in the Summer Dry Season. *Water Resour. Res.* **56** (2020).
19. WJ Hahm, et al., Bedrock vadose zone storage dynamics under extreme drought: consequences for plant water availability, recharge, and runoff. *Water Resour. Res.* (2022).

20. G Cui, Q Ma, R Bales, Assessing multi-year-drought vulnerability in dense Mediterranean-climate forests using water-balance-based indicators. *J. Hydrol.* **606**, 127431 (2022).
21. J Rungee, R Bales, M Goulden, Evapotranspiration response to multiyear dry periods in the semiarid western united states. *Hydrol. Process.* **33**, 182–194 (2019).
22. AS Jump, et al., Structural overshoot of tree growth with climate variability and the global spectrum of drought-induced forest dieback. *Glob. change biology* **23**, 3742–3757 (2017).
23. DM Rempe, WE Dietrich, Direct observations of rock moisture, a hidden component of the hydrologic cycle. *Proc. Natl. Acad. Sci.* **115**, 2664–2669 (2018).
24. L Wang-Erlandsson, et al., Global root zone storage capacity from satellite-based evaporation. *Hydrol. Earth Syst. Sci.* **20**, 1459–1481 (2016).
25. B Stocker, et al., Global distribution of the rooting zone water storage capacity reflects plant adaptation to the environment. (pre-print, 2021).
26. F Service, Record 129 million dead trees in california (2017).
27. DN Dralle, et al., Plants as sensors: Vegetation response to rainfall predicts root-zone water storage capacity in Mediterranean-type climates. *Environ. Res. Lett.* **15**, 104074 (2020).
28. ZQ Zhang, J Evaristo, Z Li, BC Si, JJ McDonnell, Tritium analysis shows apple trees may be transpiring water several decades old. *Hydrol. Process.* **31**, 1196–1201 (2017).
29. DA Lapides, WJ Hahm, DM Rempe, DN Dralle, Missing snowmelt runoff following drought explained by root-zone storage deficits. *Pre-print* (2022).
30. BC McLaughlin, et al., Hydrologic refugia, plants, and climate change. *Glob. change biology* **23**, 2941–2961 (2017).
31. KJ Fowler, et al., Towards more realistic runoff projections by removing limits on simulated soil moisture deficit. *J. Hydrol.* **600**, 126505 (2021).
32. PT La Follette, et al., Multicriteria analysis on rock moisture and streamflow in a rainfall-runoff model improves accuracy of model results. *Hydrol. Process.* p. e14536 (2022).
33. CD Jiménez-Rodríguez, M Sulis, S Schymanski, Exploring the role of bedrock representation on plant transpiration response during dry periods at four forested sites in europe. *Biogeosciences Discuss.* pp. 1–37 (2022).
34. GG Persad, DL Swain, C Kouba, JP Ortiz-Partida, Inter-model agreement on projected shifts in California hydroclimate characteristics critical to water management. *Clim. Chang.* **162**, 1493–1513 (2020).
35. DL Swain, B Langenbrunner, JD Neelin, A Hall, Increasing precipitation volatility in twenty-first-century California. *Nat. Clim. Chang.* **8**, 427–433 (2018).
36. MA Harsch, PE Hulme, MS McGlone, RP Duncan, Are treelines advancing? a global meta-analysis of treeline response to climate warming. *Ecol. letters* **12**, 1040–1049 (2009).
37. GP Asner, et al., Progressive forest canopy water loss during the 2012–2015 California drought. *Proc. Natl. Acad. Sci.* **113** (2016).
38. WRL Anderegg, et al., Hydraulic diversity of forests regulates ecosystem resilience during drought. *Nature* **561**, 538–541 (2018).
39. AG Konings, et al., Detecting forest response to droughts with global observations of vegetation water content. *Glob. Chang. Biol.* **27**, 6005–6024 (2021) _eprint: https://onlinelibrary.wiley.com/doi/pdf/10.1111/gcb.15872.
40. M Friedl, D Sulla-Menashe, Mcd12q1 modis/terra+ aqua land cover type yearly l3 global 500m sin grid v006 [data set]. *NASA EOSDIS Land Process. DAAC* **10** (2015).
41. Y Zhang, et al., Coupled estimation of 500 m and 8-day resolution global evapotranspiration and gross primary production in 2002–2017. *Remote. Sens. Environ.* **222**, 165–182 (2019).
42. C Daly, JI Smith, KV Olson, Mapping Atmospheric Moisture Climatologies across the Conterminous United States. *PLOS ONE* **10**, e0141140 (2015).
43. C Daly, et al., Physiographically sensitive mapping of climatological temperature and precipitation across the conterminous United States. *Int. J. Climatol.* **28**, 2031–2064 (2008).
44. SA Spawn, HK Gibbs, Global Aboveground and Belowground Biomass Carbon Density Maps for the Year 2010. *ORNL DAAC, Oak Ridge, Tennessee, USA* (2020).
45. TG Farr, et al., The shuttle radar topography mission. *Rev. geophysics* **45** (2007).
46. F Service, 2014-2017 forest health monitoring program aerial survey results. (2017).
47. SA Spawn, CC Sullivan, TJ Lark, HK Gibbs, Harmonized global maps of above and below-ground biomass carbon density in the year 2010. *Sci. Data* **7**, 112 (2020).
48. N Gorelick, et al., Google earth engine: Planetary-scale geospatial analysis for everyone. *Remote. Sens. Environ.* (2017).
49. S Gillies, , et al., Rasterio: geospatial raster i/o for Python programmers (2013–).
50. P Virtanen, et al., SciPy 1.0: Fundamental Algorithms for Scientific Computing in Python. *Nat. Methods* **17**, 261–272 (2020).
51. S Hoyer, J Hamman, xarray: N-D labeled arrays and datasets in Python. *J. Open Res. Softw.* **5** (2017).
52. QGIS Development Team, *QGIS Geographic Information System* (QGIS Association), (2021).
53. DN Dralle, WJ Hahm, KD Chadwick, E McCormick, DM Rempe, Technical note: Accounting for snow in the estimation of root-zonewater storage capacity from precipitation and evapotranspirationfluxes. *Hydrol. Earth Syst. Sci. Discuss.* (2020).
54. DW Pierce, DR Cayan, BL Thrasher, Statistical downscaling using localized constructed analogs (loca). *J. Hydrometeorol.* **15**, 2558–2585 (2014).
55. DW Pierce, JF Kalansky, DR Cayan, Climate, drought, and sea level rise scenarios for california's fourth climate change assessment. *California Energy Comm. California Nat. Resour. Agency* (2018).
56. CCTAG, Perspectives and guidance for climate change analysis. (2015).
57. AM Thomson, et al., RCP4.5: a pathway for stabilization of radiative forcing by 2100. *Clim. Chang.* **109**, 77–94 (2011).

Supplementary Information for

Resilience of woody ecosystems to precipitation variability

Daniella M. Rempe, Erica L. McCormick, W. Jesse Hahm, Geeta Persad, Cameron Cummins, Dana A. Lapides, K. Dana Chadwick, David N. Dralle

Daniella M. Rempe.
E-mail: rempe@utexas.edu

This PDF file includes:

Figs. S1 to S9
SI References

References

1. DM Rempe, WE Dietrich, Direct observations of rock moisture, a hidden component of the hydrologic cycle. *Proc. Natl. Acad. Sci.* **115**, 2664–2669 (2018).
2. M Friedl, D Sulla-Menashe, Mcd12q1 modis/terra+ aqua land cover type yearly l3 global 500m sin grid v006 [data set]. *NASA EOSDIS Land Process. DAAC* **10** (2015).
3. SA Spawn, HK Gibbs, Global Aboveground and Belowground Biomass Carbon Density Maps for the Year 2010. *ORNL DAAC, Oak Ridge, Tennessee, USA* (2020).
4. SA Spawn, CC Sullivan, TJ Lark, HK Gibbs, Harmonized global maps of above and belowground biomass carbon density in the year 2010. *Sci. Data* **7**, 112 (2020).
5. EL McCormick, et al., Widespread woody plant use of water stored in bedrock. *Nature* **597**, 225–229 (2021).

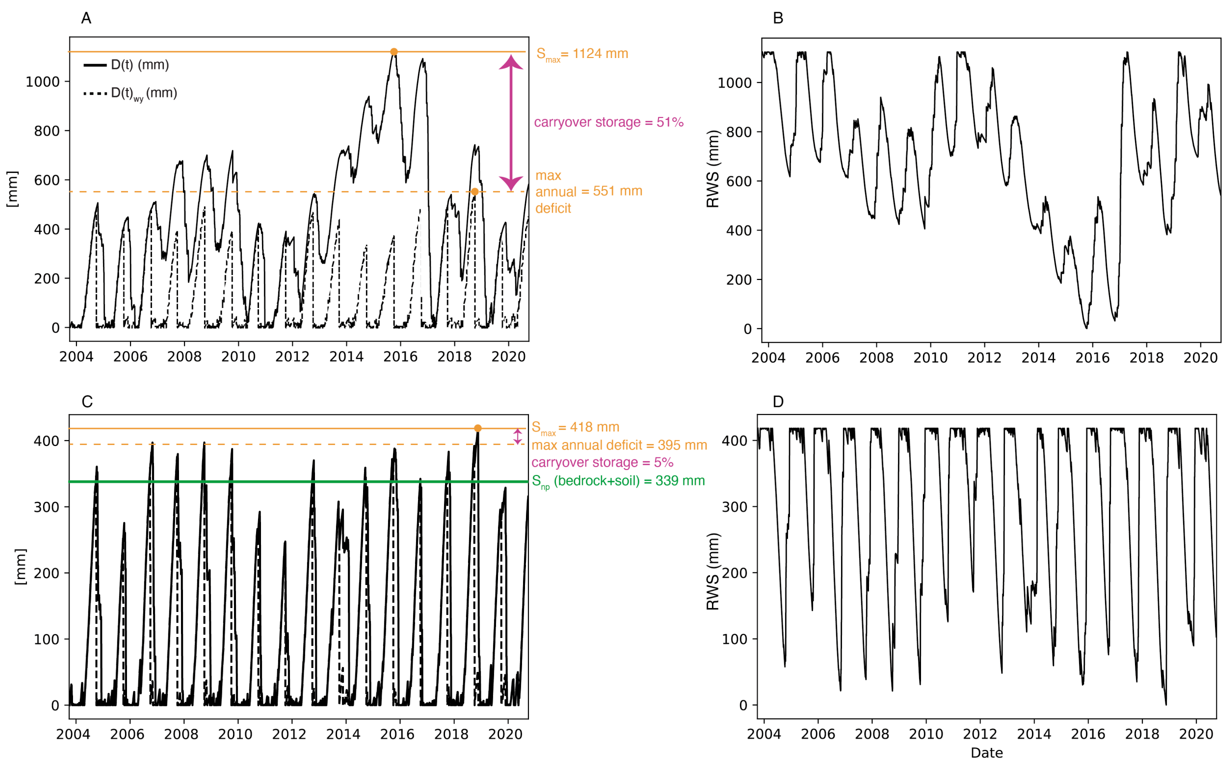

Fig. S1. Time series of deficit, $D(t)$, water year deficit, $D_{wy}(t)$, and root-water storage (RWS) from 2003 to 2020 for locations shown in Figure 1a-f. The top panel (A,B) is precipitation limited and the bottom panel (C,D) is capacity limited. Dashed line represents $D_{wy}(t)$ where deficits are reset to 0 at the start of each water year. Root-zone water storage capacity, S_{max}, is calculated as the $max(D(t)$ and designated by an orange line. The green orange line shows the maximum of $D_{wy}(t)$. Brown line shows in-situ measurements of the maximum annual deficits from soil and bedrock at the Rivendell field site reported in (1) using neutron probe (S_{np}) and soil moisture sensors. The fractional carryover storage.(C (%)) is calculated as the difference between S_{max} and $max(D(t)_{wy}$ normalized by S_{max} (see Materials and Methods). C is 51% for (A,B) and 5% for (A,C). At right, (B,D) Black line represents timevarying root-zone water storage (RWS) where the maximum value is the root-zone water storage capacity (S_{max}).

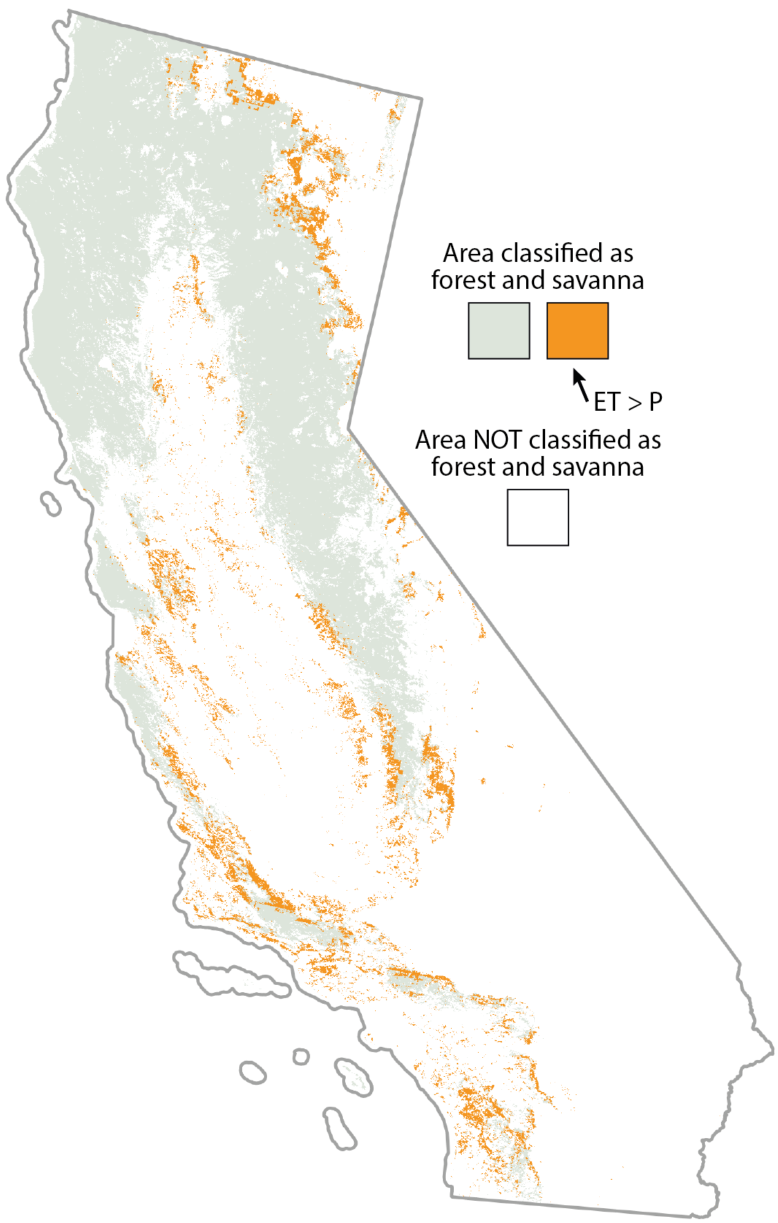

Fig. S2. Locations mapped as forested or savanna (2) where orange indicates locations which were removed because cumulative precipitation exceeds cumulative evapotranspiration (i.e. ET>P) for the years 2003 to 2020.

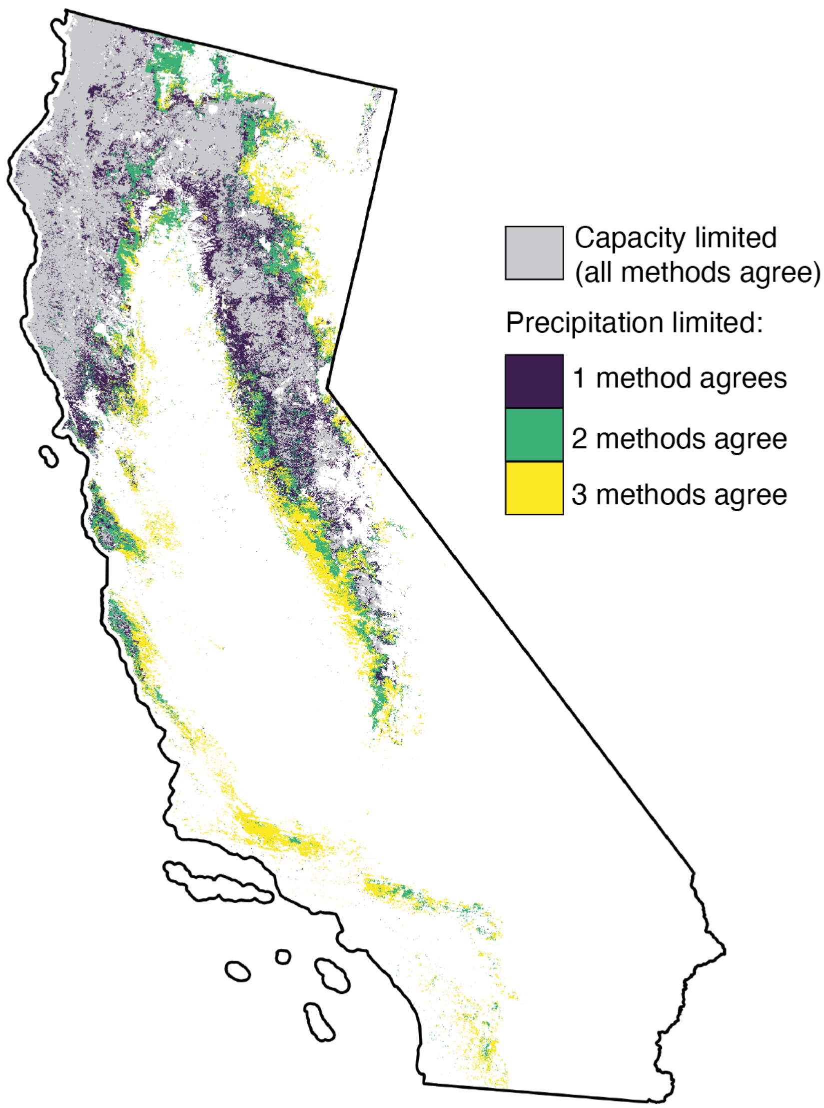

Fig. S3. Agreement between the three methods for classifying the water use of woody vegetated ecosystems as precipitation limited. Colors indicate the number of methods that agree on precipitation limitation and grey represents areas where all methods agree on capacity limitation.

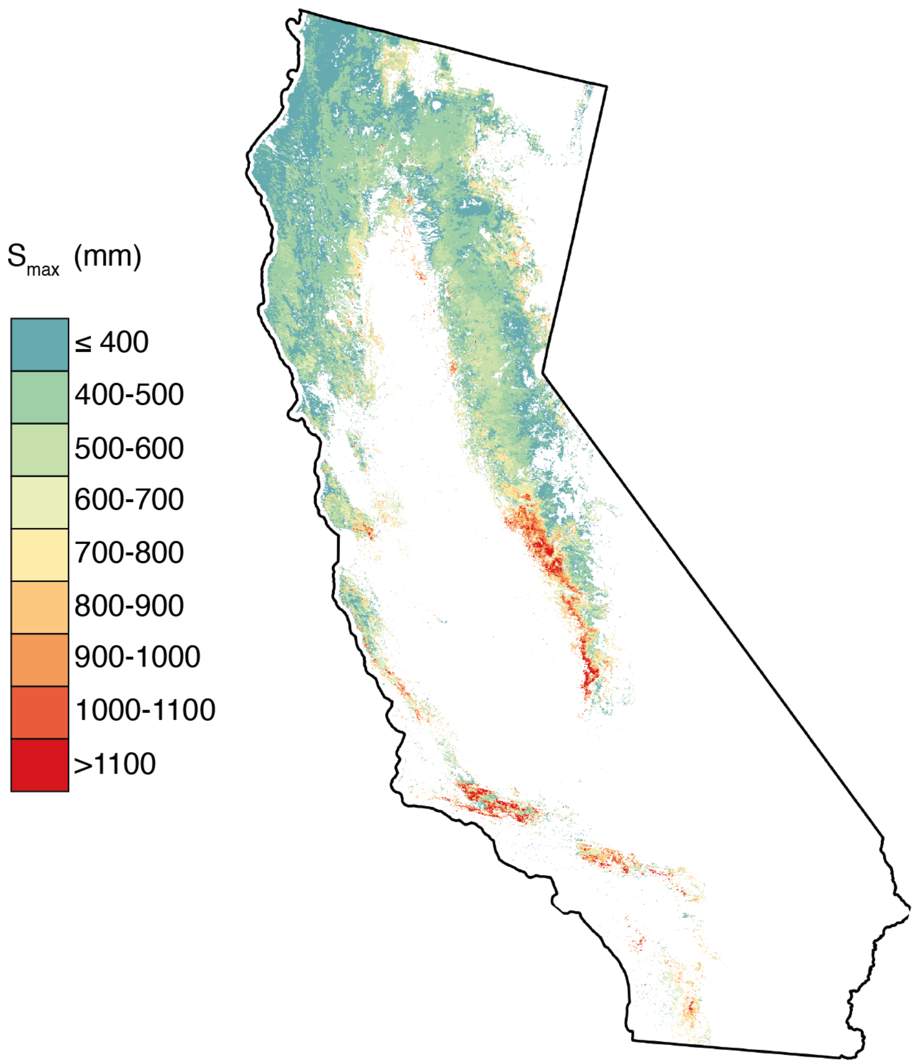

Fig. S4. Root-zone water storage capacity (S_{max}), calculated as the maximum of the root-zone water storage deficit (Figure S1, see Methods).

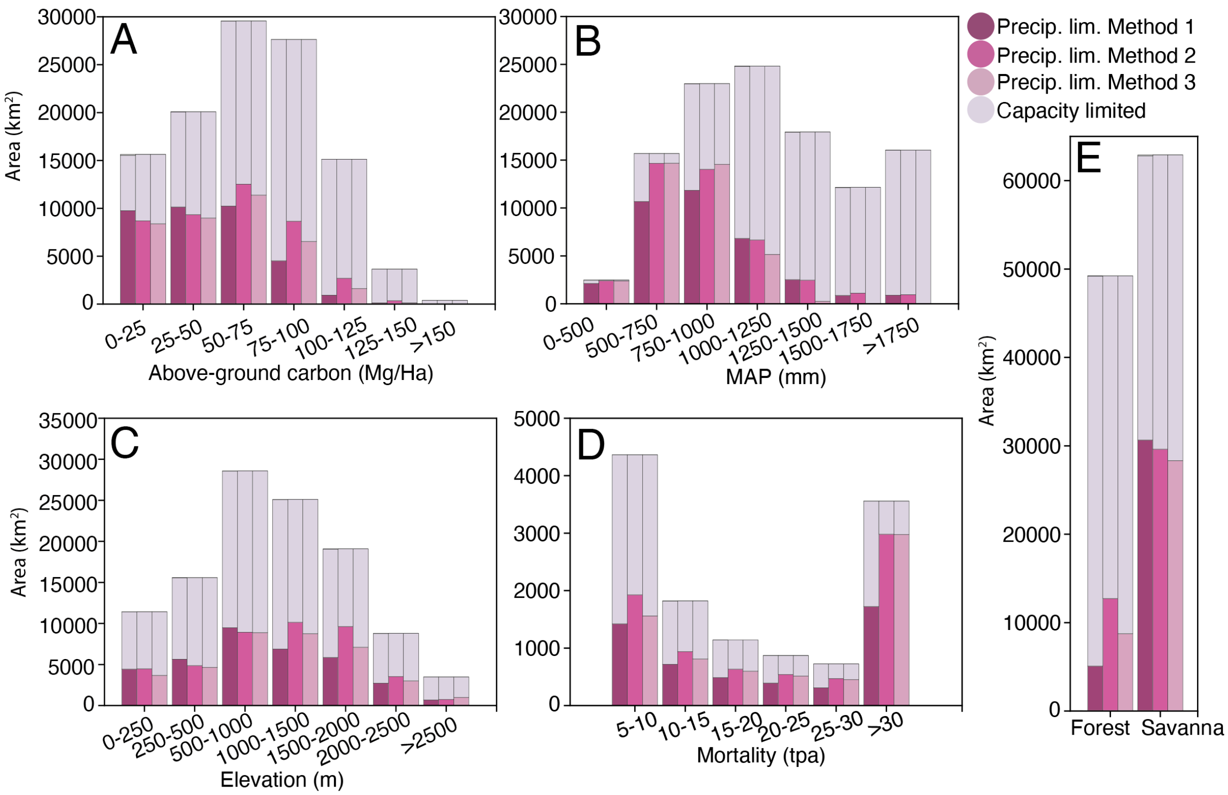

Fig. S5. The likelihood of precipitation limitation as a function of (A) above-ground carbon (3, 4), (B) mean annual precipitation (MAP), (C) elevation, (D) tree mortality from 2014 to 2017, and (E) landcover class (forest or savanna) (2). The height of each bar represents the amount of area represented by each binned class (represented as bins on the x-axis). Dark pink colors indicate the area of precipitation limitation for each class and method, respectively. The likelihood of precipitation limitation (defined as the proportion of area for each class) is shown in Figure 2. Note variable y-axis limits across subplots.

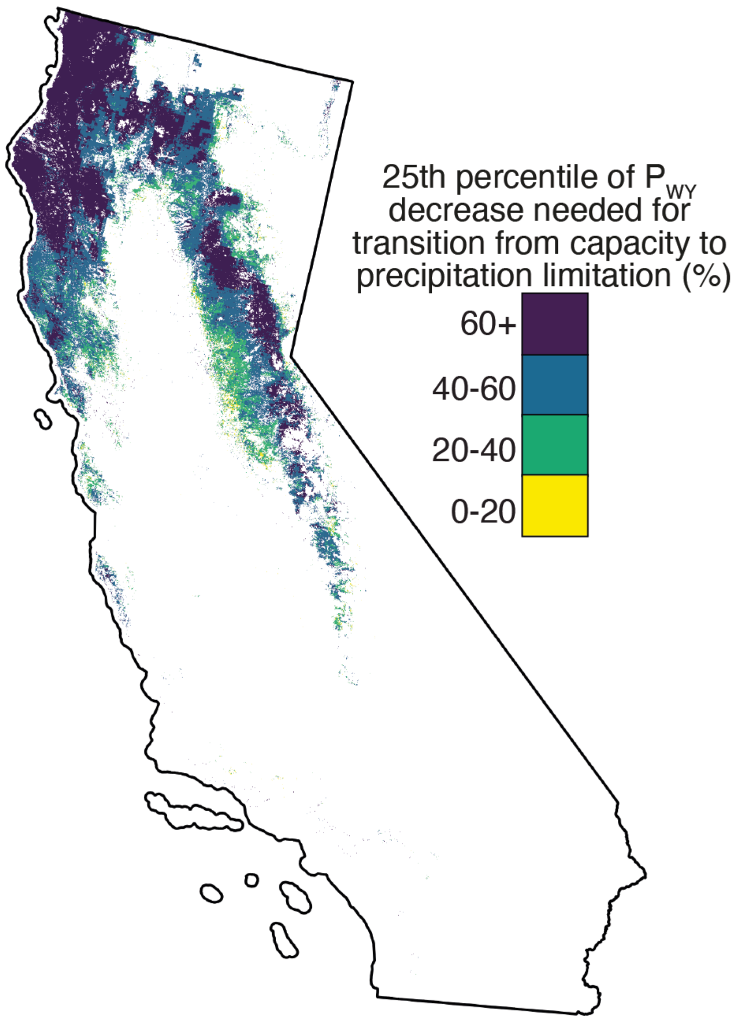

Fig. S6. Percent decrease in the 25th percentile of water year precipitation (P_{wy}) necessary to cause transition from capacity limitation to precipitation limitation according to Method 3. This map shows only areas that were categorized via Method 3 (>0% probability of S_{max}<P_{wy}) as capacity limited.

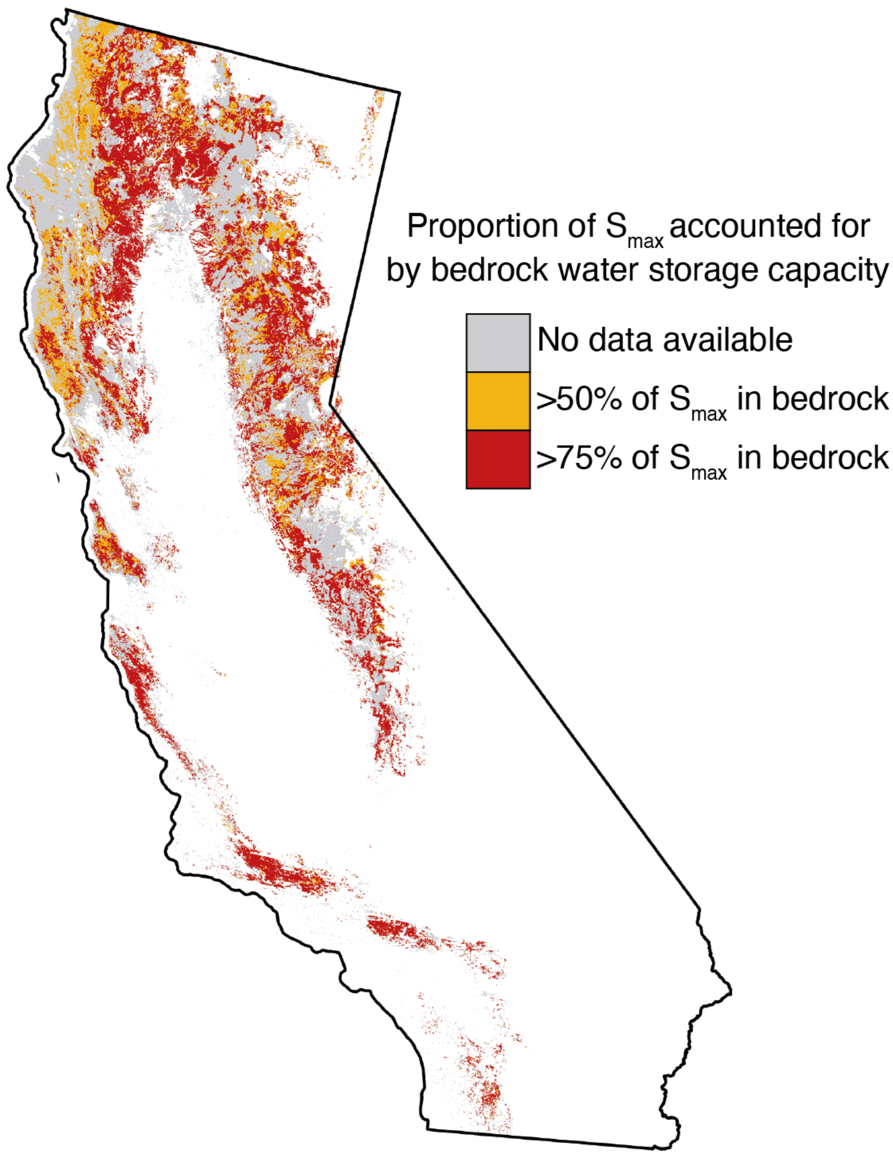

Fig. S7. The fraction of root-zone water storage capacity (S_{max}) which can be accommodated by bedrock water storage capacity. Estimates of bedrock water storage capacity from (5). Grey area represents locations included in this study which were not included in (5) and therefore do not have an estimate of bedrock water storage capacity.

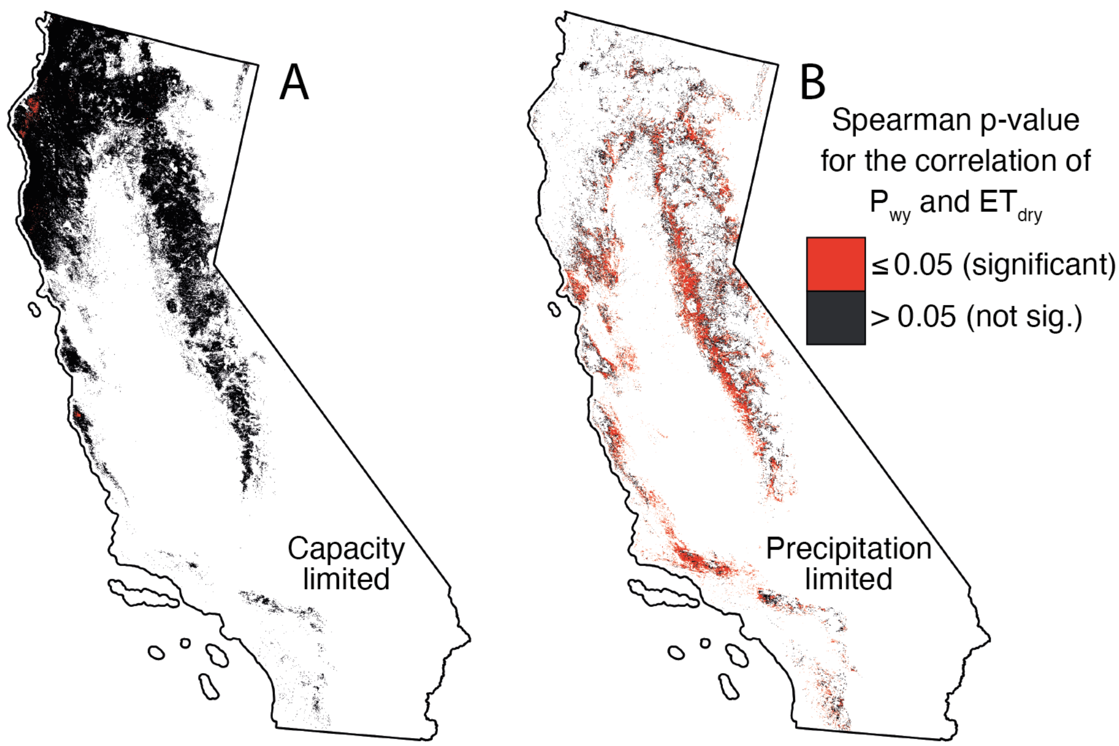

Fig. S8. Spearman p-value for the correlation between dry season evapotranspiration (ET_{dry}) and water year precipitation (P_{wy}) for regions classified as (A) storage capacity limited (B) precipitation limited according to the Spearman correlation coefficient (ρ, Method 1). Correlation coefficient (ρ) shown in Figure 1.

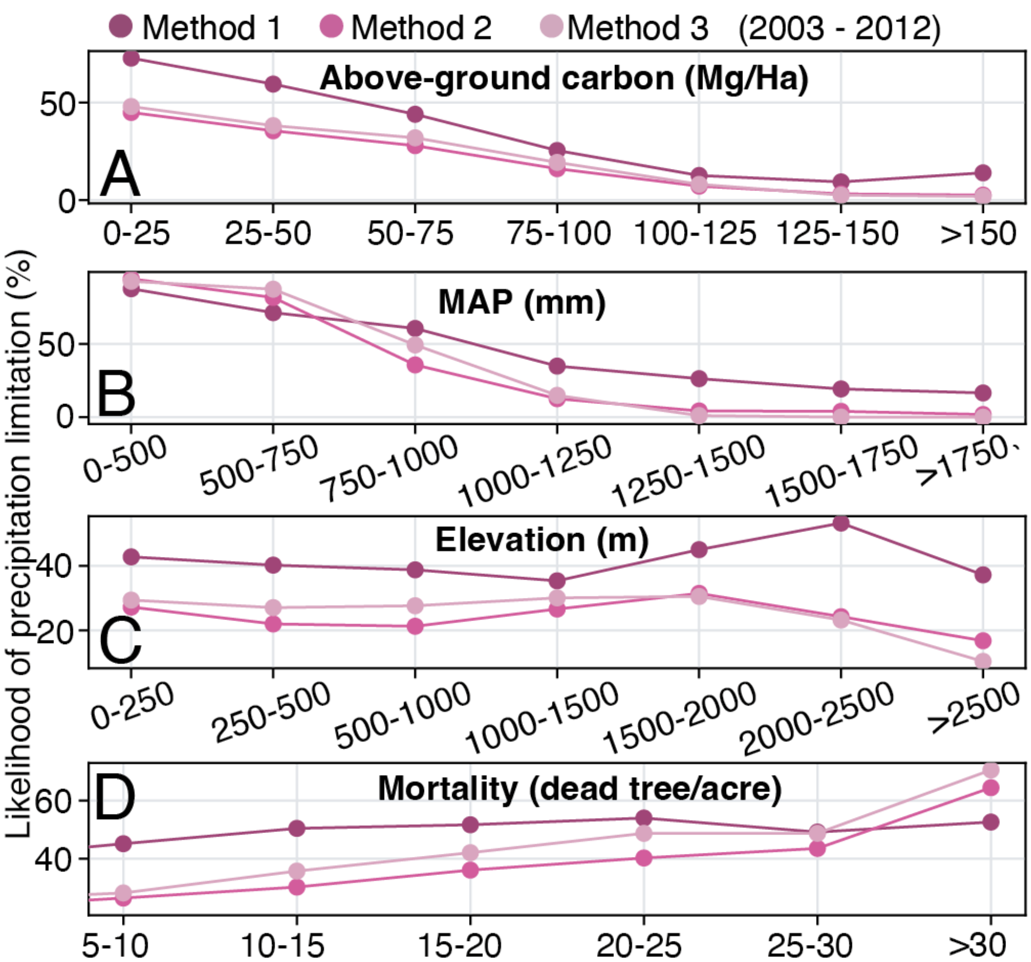

Fig. S9. The likelihood of precipitation limitation as a function of (A) above-ground carbon, (B) mean annual precipitation (MAP), (C) elevation, and (D) tree mortality from 2014-2017 (**?**) as categorized using data pre-drought data from 2003 to 2012. Likelihood is defined as the proportion of an area of a particular class (represented as bins on the x-axis) that is categorized as precipitation limited. In Figure S4, the areas of each bin are reported. This analysis is shown using the full time-series of data (2003 to 2020) in Figure 2. Note variable y-axis limits across subplots.